RSC Advances

RSC Publishing

PAPER

View Article Online
View Journal | View Issue

Cite this: *RSC Adv.*, 2013, **3**, 24126

Carrier dynamics in modulation-doped InAs/GaAs quantum rings

Chien-Hung Lin,*[a] Shin-Chin Lin,[b] Kien Wen Sun*[b] and Chien-Ping Lee[a]

Received 28th June 2013
Accepted 4th October 2013

DOI: 10.1039/c3ra43274b

www.rsc.org/advances

Carrier dynamics in undoped and modulation-doped self-assembled InAs/GaAs quantum rings was comprehensively examined through time-resolved photoluminescence techniques at room temperature. After photoexcitation, the rates of carrier capture and relaxation in the ground state and excited states were equally fast in both the undoped and charged quantum rings. Instead of cascading down through the excited states, the carriers excited in the undoped quantum rings relaxed through the quasi-continuum states *via* coupling with acoustical phonons and eventually thermalized to the ground state by emitting longitudinal optical phonons. The dynamics of carrier thermalization was governed by cold carriers in the charged quantum rings. In carrier recombination, the undoped quantum rings had a shorter PL decay time and lower luminescence intensity than the charged quantum rings because radiative recombination was suppressed by defects in the matrix and the absence of cold carriers.

I. Introduction

Zero-dimension (0D) nanostructures have been intensively studied because of their natural discrete electronic states, which expand their applications in electronics, optoelectronics and biology. Self-assembled In(Ga)As quantum dots (QDs) grown on a GaAs matrix has been one of the most exciting aspects of this research area since high-quality QDs were first created by the Stranski–Krastanov (S–K) growth mode through using molecular beam epitaxy (MBE).[1,2] Advances in epitaxial growth technology have enabled the tailoring of QDs into different geometries. In particular, In(Ga)As quantum rings (QRs) can be readily prepared through the morphological changes in In(Ga)As QDs by covering a layer of QDs with a thin GaAs cap and then carefully annealing the layer.[3–5] Given their unique ring-like reflection symmetry, QRs exhibit many interesting physical properties, such as optical nonlinearity and the Aharonov–Bohm effect,[6] and have extended applications as building blocks for optoelectronic devices such as high-speed detectors[7] and for quantum information technologies.[8,9] For those applications, optical probing of the ultrafast dynamics in nanostructure materials yields many new insights into the quantum confined behavior of excited carriers.[10–13]

In 0D systems, energetic carriers relax mostly through Auger processes at high excitation densities and through multi-phonon processes at low excitation densities.[14,15] Barker *et al.* proposed a theoretical model to describe the electron and hole wave functions in QRs.[16] They found that these wave functions have different behaviors and largely depend on the geometries and indium composition profiles associated with the strain effects and piezoelectric potentials in QRs. These parameters affect the electron–hole wave function overlapping, which results in the alternation of the optical properties of QRs. Piacente *et al.* investigated acoustic phonon-induced electron relaxation in QRs and found that electron–phonon scattering strongly relies on both lateral and vertical confinement in the ring and on the external magnetic field.[11] Both deformation potential and the piezoelectric field significantly affect the relaxation of QRs but only minimally influence that of QDs. Gomis *et al.* investigated carrier lifetimes in QR self-assembly and shape-dependent electronic structures and exciton dynamics in quantum structures of different geometries, such as dots, dashes, and camel-humps.[12] Radiative lifetimes increases with temperature because of the thermal population between the ground state (GS) and the first excited dark state.

Although undoped semiconductor nanostructures have been widely investigated and applied, they are outperformed by modulation-doped nanostructures in device applications. For example, the performance of lasers, high-speed devices, and detectors is enhanced by modulation-doped QDs.[17,18] Both vertical and lateral confinements significantly affect the room-temperature performance of optoelectronic devices based on QR structures. Therefore, understanding the relaxation and recombination dynamics of carriers in QR nanostructures is of extreme relevance. Although carrier capture and relaxation in modulation-doped QDs have been investigated,[19–21] no experiment has been conducted on carrier dynamics in the nano-ring structures.

In this paper, we report the continuous (CWPL) and time-resolved photoluminescence (TRPL) spectroscopy studies of

[a]*Department of Electronics Engineering and Institute of Electronics Engineering, National Chiao Tung University, Hsinchu, Taiwan 30010. E-mail: kb0716@gmail.com*
[b]*Department of Applied Chemistry, National Chiao Tung University, Hsinchu, Taiwan 30010. E-mail: kwsun@mail.nctu.edu.tw*

carrier capture, relaxation, and recombination in the barriers, wetting layers (WLs), excited states and GSs of undoped and modulation-doped self-assembled InAs/GaAs QRs. We describe the dependence of PL rise and decay times on cold carriers and the defects QRs matrices.

II. Samples and experiments

The samples in this study were grown on semi-insulating GaAs (001) substrates by a Varian Gen II solid-source MBE machine. QDs, which were used as precursors for QRs, were formed by S–K growth mode by depositing 2.6 monolayers of InAs at a growth rate of 0.056 μm h^{-1} at 530 °C under an As_2 atmosphere. The QDs had an average base diameter of 40 nm, a height of 10 nm, and a density of approximately 2×10^{10} cm^{-2}. To prepare QR samples, a 2 nm thin partially capping layer was deposited on the fully grown dots at a growth rate of 0.85 μm h^{-1} at 510 °C. The QD structures were annealed at the same temperature under As_2 flux for 10 seconds and subsequently transformed into QR structures. Three identical and uncoupled QR layers were sandwiched between two GaAs layers. An additional single uncapped QR layer was grown on the surface under the same growth conditions as the embedded ones for atomic force microscopy (AFM) measurements. A modulation-doped n (p) type sample with a Si (Be) delta-doped layer at 2 nm below the QR layer at a doping concentration of approximately 20 electrons (holes) per QR was prepared under the same growth conditions as the undoped QRs. The epitaxial methods are described in detail in ref. 4. Fig. 1 shows an AFM image of a QR sample. The QR samples had an area density of $\sim 2 \times 10^{10}$ cm^{-2}. The final QR shape had a base width of ~60 nm, an inner diameter of ~30 nm, a height of ~1.5 nm, and a center depth of ~1 nm.

Carrier capture and relaxation rates were determined and measured through a TRPL up-conversion technique at a time resolution of ~200 fs. Optical pulses from a self-mode-locked Ti:sapphire laser operated at a wavelength of 780 nm, duration of 150 fs, and a repetition rate of 76 MHz were used to excite carriers in the GaAs barrier. The pumping power of the laser was adjusted according to the size of the focus spot and the absorption depth at the photoexcitation wavelength to yield moderate injected carrier densities ($\sim 10^{12}$ cm^{-2}). Carrier lifetimes on a longer time scale (ns) were measured through time-correlated single-photon counting (TCSPC) technique at an overall system response of ~300 ps. A pulsed diode laser operated at a wavelength of 780 nm was used as the excitation source with pulse duration of 50 ps and a repetition rate of 80 MHz. The CWPL and TRPL signals were collected by a 0.55 m spectrometer or a 0.18 m double spectrometer and detected by a thermoelectrically-cooled InGaAs photodetector or an InGaAs photomultiplier tube.

III. Results and discussions

Fig. 2(a) shows the CWPL spectra of the three samples at high excitation power density ($\sim 3 \times 10^3$ W cm^{-2}) at 300 K. The spectral lines at 872 and 934 nm are attributed to the GaAs barrier and WL, respectively. At longer wavelengths, there are three well separated lines which represent the emissions from the confined states in the QRs. They are in the order of the GS (~1100 nm), the first excited state (1^{st} ES, ~1050 nm), and the second excited state (2^{nd} ES, ~1010 nm). The GS energy of the QRs was higher than the precursor QDs (data not shown) because of the reduced height and the enhanced vertical confinement from the ring shape. By constrast, the energy

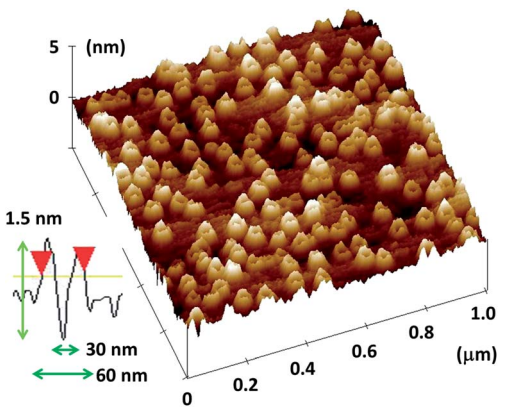

Fig. 1 AFM image of the QRs with a scanning area of 1 × 1 μm^2. The inset shows the cross-section morphology of the ring which gives an outer diameter of ~60 nm, inner diameter of ~30 nm, and center depth of ~1.5 nm.

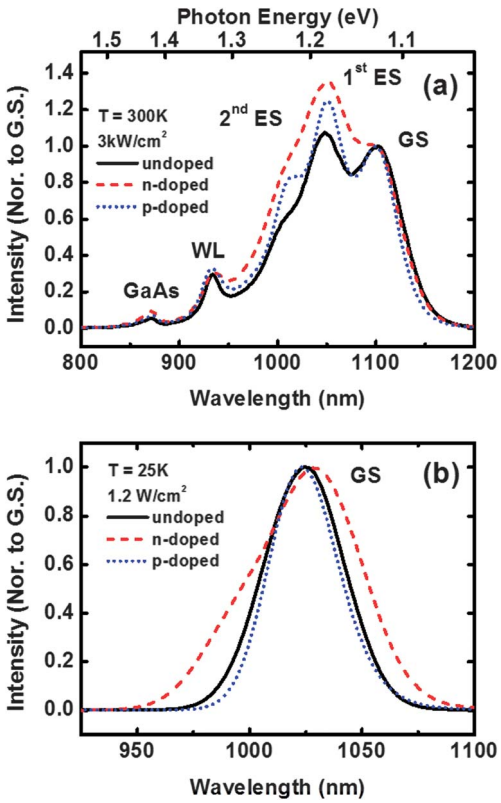

Fig. 2 CWPL spectra of undoped (black solid line), n-doped (red dash line), and p-doped QRs (blue dot line) at (a) high excitation power density and 300 K and (b) low excitation power density and 25 K. Each luminescence spectrum is normalized to the GS.

difference (~55 meV–60 meV) between the confined states in the QRs was slightly reduced compared with that in the QDs (~70 meV) because of the increased base diameters of the rings. The three QR samples revealed similar CWPL properties except that a slightly higher PL intensity was observed from the excited states of the modulation-doped rings. This result indicates that the geometries of the doped and undoped QR samples were almost alike. Fig. 2(b) shows the CWPL spectra of the samples at low temperature and low excitation power density (~1.2 W cm^{-2}). The undoped QR spectrum, which can be fitted with a single Gaussian distribution, exhibited a full width at half-maximum (FWHM) of 50 meV and indicated the uniform size distribution of the rings. The bandgap of the QD GS is altered by doping-induced inter-diffusion.[19,20,22] Excess carriers in the n-(p-)doped QDs induced the red (blue) shift of GS energy compared with those in the undoped QDs. A slight blue shift (~2 meV) in GS energy was also observed among the p-doped QRs and a red shift (~5 meV) among the n-doped QRs. However, these changes in GS energy were not as significant as reported in ref. 19, 20 and 22 probably because the post-annealing processes during QR growth reduced the inter-diffusion effect. Therefore, GS energy was only slightly modified.

To study carrier capture and relaxation in the QRs, we focused on the initial rising part of the TRPL spectra in Fig. 3. The TRPL spectra of the barrier, WL, 1st ES, and GS of the undoped QRs were detected at fixed energies determined from the CWPL measurements (Fig. 3(a)). The sample was excited at 1.59 eV (above the barrier) at 300 K with a moderate excitation power density of ~240 W cm^{-2}, which corresponds to an area density of 3.2×10^{12} electron–hole pairs per cm^2. The rising feature of the spectrum of the GaAs barrier indicates that carrier rapidly cooled and thermalized within the barrier on a sub-ps time scale (0.4 ps).[20] A similar tendency was observed in both the undoped and charged QRs. The initially excited carriers in the GaAs barrier were subsequently transported and captured into the WL and QRs as indicated by the steep edge of the PL transients of the WL, 1st ES, and GS. Note that the edge of the 1st ES rose more slowly than those of the barrier and WL; however, it was comparable to that of the GS.

Fig. 3(b) shows the PL transients detected at the GSs of the undoped and charged QRs at moderate excitation density. Rise time τ_r can be measured by fitting the rising edge of the PL transients with the following rate equation: $I(t) \propto [1 - (e^{-t/\tau_r})]$. The normalized CWPL spectra of the undoped, n-doped, and p-doped QRs at moderate excitation power density and 300 K are displayed in Fig. 3(c). The rise times of all states for both the undoped and charged samples are summarized in Fig. 4(a). Siegert *et al.*[20] found that the rise time of the WL in the undoped and doped QDs is in the order of ~2 ps. The ultrafast capture time, which is shorter than the estimated ambipolar diffusion time in the WL, is attributed to a long-range attractive potential induced by strain in the QDs. Although the built-in carriers in the charged QDs introduce potential variations and a built-in field around the QDs, the cold carriers in the charged QDs only minimally affects the carrier transport in the barrier. However, a remarkable difference in WL capture time was found between the undoped (~3 ps) and charged (~1 ps) QRs in our

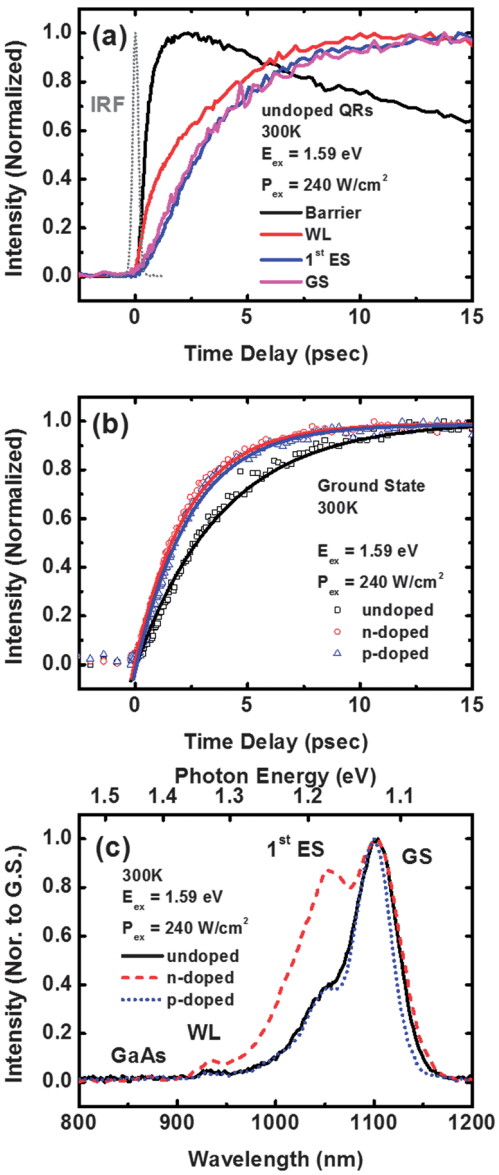

Fig. 3 (a) Normalized TRPL spectra measured at energies of the GaAs barrier, WL, 1st ES, and GS of the undoped QRs at moderate excitation power density and 300 K. IRF indicates the instrumental response function and zero delay. (b) The TRPL spectra of the GSs for the undoped (black squares), n-doped (red circles), and p-doped QRs (blue triangles). (c) Normalized CWPL spectra of undoped (black solid line), n-doped (red dash line), and p-doped QRs (blue dot line) at moderate excitation power density and 300 K.

experiments. In the ring geometry, the potential variation and field induced by the built-in cold carriers accelerated the transport and capture rates in the WL.[22] We speculated that the enhanced vertical confinement (~1.5 nm) increased the strength of the screening polarization field (potential variation) induced by the charges localized (doped) in a QR.

The carrier capture and relaxation in the discrete states of the 0D nanostructures were dominated by two major mechanisms. At low to moderate excitation levels (10^9 cm^{-2} to 10^{12} cm^{-2}), the energetic carriers in the WL can relax toward the discrete states by a single optical phonon emission or multi-phonon (optical and acoustic phonon) emissions. By

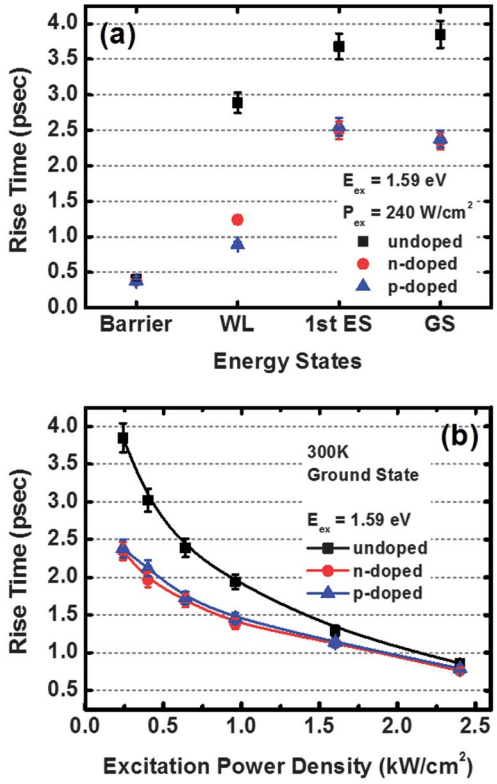

Fig. 4 (a) Rise times extracted from the TRPL transients for undoped (black squares), n-doped (red circles), and p-doped QRs (blue triangles) at moderate excitation power density and 300 K. (b) Power density dependence of the rise times in the GSs of the doped and undoped QRs.

contrast, carrier–carrier scattering transfers one carrier into a lower-energy state and excites the other to a higher-energy state; this phenomenon is known as the Auger process and is common at high excitation levels (>10^{12} cm^{-2}). At an excitation level of ~10^{12} cm^{-2}, a rise time of ~3.7 ps was obtained for the excited state in the undoped QRs, and ~2.5 ps was derived in the charged QRs. These numbers agree with QD carrier capture measurements,[20,23] which range from 1 ps to 10 ps. Increasing excitation power density decreased the rise times of the GSs in both the undoped and charged QRs (Fig. 4(b)). At an excitation density above ~3.2 × 10^{13} cm^{-2}, the PL rise times of both the undoped and charged QRs were below 1 ps and thus began to saturate.

We evaluated the "net" carrier capture time of the 1st ES by subtracting the rise time of the excited state from the WL rise time and found the results of the excited states were almost identical to those of the GS in both the undoped and charged QRs. A slightly shorter "net" capture time (~0.8 ps) was also obtained in the excited state of the undoped QRs than in the excited state of the n- (~1.2 ps) and p-doped (~1.6 ps) QRs. The similar capture times in all QR discrete levels in the undoped samples seemed unusual. Carrier capture and relaxation between discrete levels in confined systems often follow a natural cascade process, as indicated in the different PL rise times in different levels.[24] In the charged QRs (with a moderate doping density of 10^{12} cm^{-2} or higher), carrier–carrier or Auger scattering induced by the built-in carriers enhanced carrier capture and intralevel relaxation and resulted in comparable PL rise times between different discrete states. Therefore, the rise times were about equal in all QR discrete levels in our doped samples. However, the absence of cold carriers (*i.e.* of carrier–carrier or Auger scattering) in our undoped sample made the PL rise times between the discrete levels not only equally fast but also comparable to or even faster than those in the charged samples. This result implies that the excited states in the QRs no longer mediated cascade relaxation. Another relaxation mechanism facilitated the fast relaxation of carriers into the excited state and GS.

Fig. 5 shows the PL and Photoluminescence excitation (PLE) spectra of the QRs at 1.4 K. The PLE spectrum of the undoped sample showed a resonance peak at 70 meV above the GS energy and was accompanied by a continuum background. The resonance peak is attributed to the 1st ES ($n = 0$, $l = 1$) of the undoped QRs. This result was confirmed by magnetic field-dependent PLE measurements, in which the level reveals an energy splitting of about 34 meV at 14 Tesla (data not shown).[25] However, only a featureless continuum background was observed in the PLE spectra for the doped sample because of the band-filling effect of the built-in cold carriers. This, or quasi-continuum state is an absorption spectrum of the cross-transition from the delocalized state to the bound state, such as the recombination of a WL hole with a GS electron (WLh–1Se) or of a GS hole recombined with a WL electron (1Sh–WLe). The continuum background provides an efficient channel for carriers to relax into lower states by coupling with longitudinal acoustical (LA) phonons.[26–28] The extension of the quasi-continuum state further below the 1st ES enables photoexcited carriers to couple with LA phonons *via* the quasi-continuum state; this capacity remains until the remnant energy of the carriers equals the longitudinal optical (LO) phonon energy and then thermalizes into the GS by LO phonon emission.[29] Relaxation time is expected to be shorter than 1 ps in single LO phonon emission process at a photoexcited carrier density of 10^{12} cm^{-2} or less.[30] The GSs of our samples were close to the

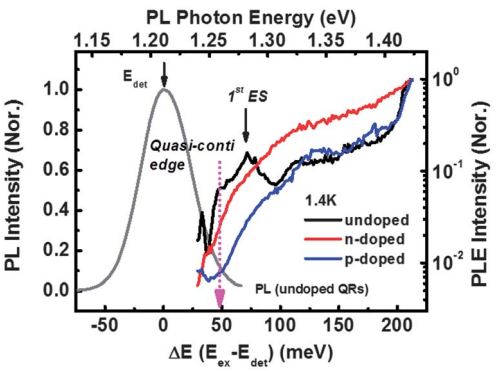

Fig. 5 Normalized PLE spectra of undoped (black line), n-doped (red line), and p-doped QRs (blue line) as a function of relaxation energy ($E_{exc} - E_{det}$) recorded at 1.4 K and $E_{det} = 1.211$ eV. Each PLE spectrum is normalized to the intensity of the heavy-hole to WL transition. The gray curve shows the PL spectrum of the undoped QRs excited at 1.4 K.

onset of the quasi-continuum background (indicated by an arrow in Fig. 5) because of the increased vertical confinement and bandgap of the QRs. Similar results have been reported in PLE studies of small QDs.[31] In our experiments, the observed short and comparable PL rise times between discrete levels can be interpreted and supported by the above relaxation channel.

To investigate the effect of doping on carrier lifetimes in the QRs, PL signals of the GSs were studied through TCSPC at low excitation densities and on a longer time scale (ns). The time-resolved spectra are shown in Fig. 6(a). The overall carrier lifetime τ, including radiative term and non-radiative terms, can be expressed by $\tau = \frac{\tau_r \tau_{nr}}{\tau_r + \tau_{nr}}$, where τ_r and τ_{nr} represent the radiative and non-radiative lifetimes, respectively. The non-radiative term originates from sample defects, which act as efficient recombination centers.

The initially excited carriers after capture and relaxation in the GS, quickly recombined with the cold electrons (holes) at the bottom of the conduction (valence) band in the n-(p-)doped QRs and radiatively lost their energy. The p-doped QR sample had a slightly longer lifetime than the n-doped one because the photoexcited holes relaxed more rapidly than the electrons. In general, the carrier lifetimes in undoped QRs should be longer than those in charged ones because of the absence of cold carriers. However, in contrast to earlier reports on QDs,[20] our undoped sample revealed a shorter PL decay time (~0.3 ns) at 300 K than the charged QRs (Fig. 6(a)). The longer lifetimes of the charged QRs at room temperature imply a lower non-radiative recombination rate. Therefore, stronger light emission is expected. Fig. 6(b) shows the unnormalized CWPL of all samples at 300 K under the same excitation conditions. The charged QRs had higher luminescence intensity than the undoped ones. Unlike in the undoped QRs, the cold carriers in the doped QRs suppressed the non-radiative mechanism and strengthened light emission.

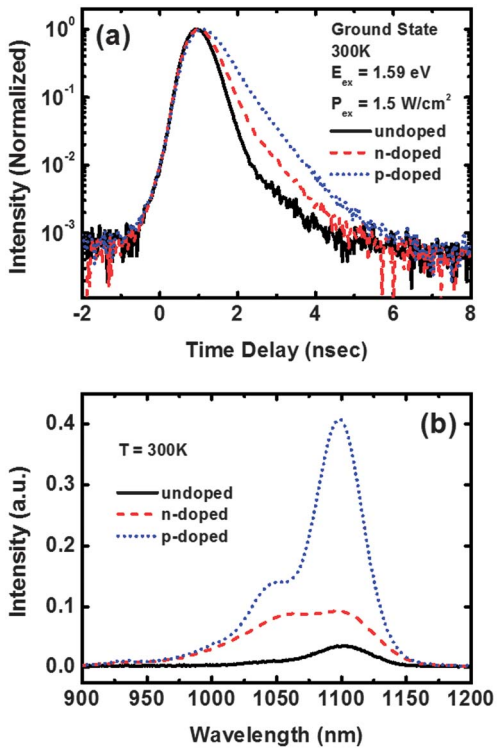

Fig. 6 (a) Normalized TRPL spectra in the GS of undoped (black solid line), n-doped (red dash line), and p-doped QRs (blue dot line) at 300 K. (b) Unnormalized CWPL spectra of undoped, n-doped, and p-doped QRs at low excitation power density and 300 K.

IV. Conclusions

We presented PL transient studies of MBE-grown undoped, p-doped, and n-doped QR nanostructures. At moderate excitation power density, carrier capture and relaxation in the excited and GS of the three QRs were carefully examined. The carriers excited in the GaAs were rapidly captured and thermalized in the WL on a sub-ps time scale in both the undoped and charged QRs. In the charged QRs, carrier–carrier or Auger scattering induced by built-in carriers enhanced carrier capture and intra-level relaxation and resulted in comparable PL rise times between different discrete levels. The intraband optical properties of the QRs were also affected by the crossed electron–hole levels (*i.e.*, the quasi-continuum states). The cold carriers suppressed the non-radiative mechanism and strengthened light emission in the charged QRs. The successful demonstration of high-performance lasers and high-speed devices using p-doped QDs confirms that charged QRs with ultrafast carrier capture time and low non-radiative recombination rate are excellent materials.

Acknowledgements

This study was supported by the National Science Council of the Republic of China (Grant no. NSC 99-2119-M-009-004-MY3) and by the Aim for the Top University (ATU) program of the Ministry of Education of Taiwan.

References

1 M. Tabuchi, S. Noda and A. Sasaki, *Science and Technology of Mesoscopic Structures*, Springer-Verlag, Tokyo, Japan, 1992.
2 J. Y. Marzin, J. M. Gerard, A. Izrael, D. Barrier and G. Bastard, *Phys. Rev. Lett.*, 1994, **73**, 716.
3 A. Lorke, R. Johannes Luyken, J. M. Garcia and P. M. Petroff, *Jpn. J. Appl. Phys., Part 1*, 2001, **40**, 1857.
4 H. S. Ling and C. P. Lee, *J. Appl. Phys.*, 2007, **102**, 024314.
5 J. Wu, Z. M. Wang, K. Holmes, E. Marega, Z. Zhou, H. D. Li, Y. I. Mazur and G. I. Salamo, *Appl. Phys. Lett.*, 2012, **100**, 203117.
6 M. Grochol, F. Grosse and R. Zimmermann, *Phys. Rev. B: Condens. Matter Mater. Phys.*, 2006, **74**, 115416.
7 S. Bhowmick, G. Huang, W. Guo, C. S. Lee, P. Bhattacharya, G. Ariyawansa and A. G. U. Perera, *Appl. Phys. Lett.*, 2010, **96**, 231103.
8 *Semiconductor Spintronics and Quantum Computation*, ed. D. D. Awschalom, D. Loss and N. Samarth, Springer, Berlin, 2002.

9 T. Koga, J. Nitta, T. Akazaki and H. Takayanagi, *Phys. Rev. Lett.*, 2002, **89**, 046801.
10 U. Bockelmann and G. Bastard, *Phys. Rev. B: Condens. Matter Mater. Phys.*, 1990, **42**, 8947.
11 G. Piacente and G. Q. Hai, *Phys. Rev. B: Condens. Matter Mater. Phys.*, 2007, **75**, 125324.
12 J. Gomis, J. Martinez-Pastor, B. Alen, D. Granados, J. M. Garcia and P. Roussignol, *Eur. Phys. J. B*, 2006, **54**, 471.
13 C. H. Lin, H. S. Ling, C. C. Huang, S. K. Su, S. D. Lin, K. W. Sun, C. P. Lee, Y. K. Liu, M. D. Yang and J. L. Shen, *Appl. Phys. Lett.*, 2009, **94**, 183101.
14 D. Morris and N. Perret, *Appl. Phys. Lett.*, 1999, **75**, 3593.
15 R. Heitz, M. Veit, N. N. Ledentsov, A. Hoffmann, D. Bimberg, V. M. Ustinov, P. S. Kop'ev and Zh. I. Alferov, *Phys. Rev. B: Condens. Matter Mater. Phys.*, 1997, **56**, 10435.
16 J. A. Barker, R. J. Warburton and E. P. O'Reilly, *Phys. Rev. B: Condens. Matter Mater. Phys.*, 2004, **69**, 035327.
17 P. Bhattacharya, D. Klotzkin, O. Qasaimeh, W. Zhou, S. Krishna and D. Zhu, *IEEE J. Sel. Top. Quantum Electron.*, 2000, **6**, 426.
18 O. B. Shchekin and D. G. Deppe, *Appl. Phys. Lett.*, 2002, **80**, 3277.
19 K. Gündoğdu, K. C. Hall, T. F. Boggess, D. G. Deppe and O. B. Shchekin, *Appl. Phys. Lett.*, 2004, **85**, 4570.
20 J. Siegert, S. Marcinkevičius and Q. X. Zhao, *Phys. Rev. B: Condens. Matter Mater. Phys.*, 2005, **72**, 085316.
21 K. W. Sun, A. Kechiantz, B. C. Lee and C. P. Lee, *Appl. Phys. Lett.*, 2006, **88**, 163117.
22 O. B. Shchekin, D. G. Deppe and D. Lu, *Appl. Phys. Lett.*, 2001, **78**, 3115.
23 J. Feldmann, S. T. Cundiff, M. Arzberger, G. Böhm and G. Abstreiter, *J. Appl. Phys.*, 2001, **89**, 1180.
24 T. Müller, F. F. Schrey, G. Strasser and K. Unterrainer, *Appl. Phys. Lett.*, 2003, **83**, 3572.
25 The energy splitting of 0D nanostructures in magnetic field was demonstrated by Zeeman splitting and diamagnetic shift, $\Delta E(B) = E_{\text{Zeeman}} + E_{\text{dia}} \approx E_{\text{Zeeman}} = \frac{m_l e^h/2\pi}{2m^*}B$. Set $m^* \sim 0.05m_0$, $\Delta E(B) \sim 33$ meV at 14 Tesla.
26 Y. Toda, O. Moriwaki, M. Nishioka and Y. Arakawa, *Phys. Rev. Lett.*, 1999, **82**, 4114.
27 C. Kammerer, G. Cassabois, C. Voisin, C. Delalande and Ph. Roussignol, *Phys. Rev. Lett.*, 2001, **87**, 207401.
28 A. Vasanelli, R. Ferreira and G. Bastard, *Phys. Rev. Lett.*, 2002, **89**, 216804.
29 E. W. Bogaart, J. E. M. Haverkort, T. Mano, T. van Lippen, R. Nötzel and J. H. Wolter, *Phys. Rev. B: Condens. Matter Mater. Phys.*, 2005, **72**, 195301.
30 I. Magnusdottir, A. V. Uskov, S. Bischoff, B. Tromborg and J. Mørk, *J. Appl. Phys.*, 2002, **92**, 5982.
31 C. I. Shih, C. H. Lin, S. C. Lin, T. C. Lin, K. W. Sun, O. Voskoboynikov, C. P. Lee and Y. W. Suen, *Nanoscale Res. Lett.*, 2011, **6**, 409.